ACS OMEGA

http://pubs.acs.org/journal/acsodf

Article

Nuclear Magnetic Relaxation Mapping of Spin Relaxation in Electrically Stressed Glycerol

Adam D. Wexler, Jakob Woisetschläger, Ursula Reiter, Gert Reiter, Michael Fuchsjäger, Elmar C. Fuchs,* and Lothar Brecker

Cite This: https://dx.doi.org/10.1021/acsomega.0c02059

Read Online

ACCESS | Metrics & More | Article Recommendations

ABSTRACT: This work discusses nuclear magnetic relaxation effects in glycerol subject to a strong electric field. The methods used are 1.5 T magnetic resonance imaging (MRI), referenced by 9.4 T nuclear magnetic resonance (NMR). While MRI allows a glycerol probe to be sampled with a high voltage (HV) of 16 kV applied to the probe, NMR provides precise molecular data from the sample, but the sample cannot be tested under HV. Using MRI, the recording of magnetic relaxation times was possible while HV was applied to the glycerol. NMR spectroscopy was used to confirm that MRI provides a reasonably accurate estimation of temperature. The applied HV was observed to have a negligible effect on the spin−lattice relaxation time T_1, which represents the energy release to the thermal bath or system enthalpy. In contrast to that, the spin−spin relaxation time T_2, which does represent the local entropy of the system, shows a lower response to temperature while the liquid is electrically stressed. These observations point toward a proton population in electrically stressed glycerol that is more mobile than that found in the bulk, an observation that is in agreement with previously published results for water.

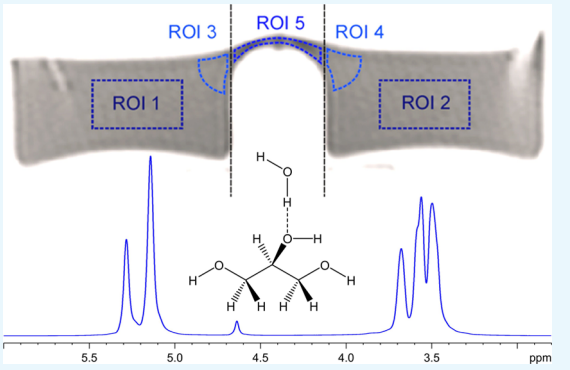

1. INTRODUCTION

The electrohydrodynamics (EHDs) of polar liquids exposed to strong electric fields (up to ~10^6 V m^{-1}) have been studied extensively. Hertz[1] was one of the first to note the rotational motion in liquid−solid dielectric systems, Quincke[2] observed that the interfacial tension between two fluids was changed by the application of an external electric field and a subsequent exertion of forces on the fluid body inducing rotational motion, and Armstrong[3] discovered the so-called "floating water bridge" in 1893. The floating water bridge is a horizontal EHD bridge forming between two beakers filled with deionized water when a high direct current (DC) voltage is applied. The experimental configuration allows proton conduction and diffusion processes to occur as would normally occur while the liquid is exposed to air under ambient conditions while also reducing the possibility of a dielectric breakdown induced by the applied potential.

Recently, a phase transition in electrically stressed liquid water was reported, whereby the breakdown of rotational symmetry in the molecular dipole results in a dipole polarization current, which propagates along the hydrogen bond network. The emergence of the novel phase is described using quantum field theory demonstrating that electric fields of this magnitude generate nontrivial material transitions.[4,5] While these experiments were performed in deionized water without any EHD flow or free charge carriers, the horizontal EHD bridges offer the possibility to test the influence of electric fields on polar liquids under more relevant conditions for engineering or biology. In these aqueous bridges, an increased positive surface charge was found, leading to a decrease in surface tension by app. 4%.[6,7]

The question now arises whether and how electric fields of such strength can alter physical properties in liquids made of polar molecules other than water. Nonaqueous liquid bridges have been previously investigated for other polar molecules, namely, methanol, ethanol, 1-propanol, 2-propanol, glycerol, and dimethyl sulfoxide (DMSO).[8−12] In DMSO, an aprotic liquid, ionized molecules like O_2 are suggested to act as charge carriers,[11] whereas in protic liquids, e.g., water, protons have been identified to fulfill this purpose. The alcohol group protons in glycerol are expected to behave in a similar fashion to those in water, which were found to be more delocalized and more mobile in electrically stressed water than in bulk

Received: May 4, 2020
Accepted: August 6, 2020

water.[13] In this work, the enhanced delocalization of protons in electrically stressed glycerol is investigated by nuclear magnetic resonance (NMR) and magnetic resonance imaging (MRI) in terms of spin−spin relaxation time (T_2) and spin−lattice relaxation time (T_1) measurements.

This was done for three reasons:

(1) The T_1 relaxation time of glycerol (~53 ms) is much shorter than that of water (~2700 ms) at 1.5 T used for MRI[14] such that the acquisition times for relaxation time measurements can be shortened.

(2) The higher viscosity of glycerol (1.412 Pa·s)[15] than of water (8.9×10^{-4} Pa·s)[16] potentially reduces the influence of motion artifacts on the resulting relaxation time maps.

(3) Upon dissociation of protons from hydroxyl groups (OH groups), the remaining glycerol backbone contains additional distinguishable alkyl protons, which allow a separate NMR spectroscopic analysis of these moieties.

NMR spectroscopy is a common tool for molecular structure and dynamics analysis[17] and can serve in the present study as a benchmark for the MRI recordings of operating glycerol bridges. Therefore, the objective of this study is to test the hypothesis that moderately strong electric fields have an influence on the properties of polar protic molecules other than water.

2. BACKGROUND

2.1. Electrohydrodynamic Bridges in Polar Liquids. The fluid motion in an electrically stressed liquid composed of polar molecules is governed by the laws of both hydrodynamics and electrodynamics whose combination is referred to as electrohydrodynamics or electro-fluid-dynamics.[18,19] In this approach, an additional term enters the Bernoulli equation for an electrically stressed, adiabatic, and incompressible liquid, the so-called Maxwell pressure. When the HV applied to the liquid is large enough, this EHD pressure may counteract the hydrostatic pressure, so that an electrically stressed polar liquid moves upward, against gravity.[20]

Experiments with EHD bridges were performed for several decades,[21,22] but only recently, a century-old experiment in electrically stressed water has been rediscovered.[23] First proposed by Lord Armstrong in 1893,[3] this experiment presents a horizontal EHD bridge, often referred to as the floating water bridge. The electrochemistry of such a horizontal EHD liquid water bridge has been investigated[24] describing the bridge as a protonic semiconducting liquid. Generated in the anolyte by HV electrolysis, protons are transported to the catholyte through the water bridge, which acts as an Ohmic resistor limiting the current in this HV experiment. In the bridge, the protons cause a nonthermic infrared (IR) emission.[25] If the bridge is broken abruptly, the system is taken out of its electrochemical equilibrium, and excess protons and *ater*-protons (proton holes in the liquid) remain in the beakers, producing charged water with altered physical properties relevant for engineering, such a reduced surface tension as previously mentioned.[6,7] Details about how to safely build and run an EHD bridge setup are discussed elsewhere.[26]

Horizontal aqueous EHD bridges have recently provided insights into the molecular physics of electrically stressed water because these bridges are both large and stable enough to be used in experiments that access the molecular length scale and also require a macroscopic sample volume, e.g., radiation scattering[27−31] and spectroscopy.[25,32] Previous Raman studies reported a small fraction of molecules in electrically stressed water to be dynamically polarized,[33,4] a state where the O−H vibrations quantum-mechanically couple and hydrogen bonds are strengthened.[5,32]

2.2. Magnetic Resonance Principles Used in the Present Study. NMR spectroscopy is an analytical method to investigate the electronic environment of individual atomic nuclei as well as their interactions with atomic nuclei of adjacent atoms. It enables structure elucidation of molecules and investigation of molecular dynamics behavior. The method is based on magnetic nuclear resonance, a resonant interaction between the magnetic moment of atomic nuclei located in a strong static magnetic field, with a high frequency electromagnetic irradiation. Only these isotopes are detectable, which have a nonzero nuclear spin in the ground state and thus possess a magnetic moment (μ).

In simple words, such atomic nuclei are charge carriers possessing a rotating nuclear spin. Their magnetic moment (μ) can assume only certain quantum-mechanically defined orientations in an external magnetic field. The number of possible orientations is determined by the nuclear spin quantum number I. For each nuclear spin quantum number I, there are $2I + 1$ orientations and each orientation is assigned a magnetic nuclear spin quantum number m_I. Protons (in hydrogen atoms) that have $I = {}^1/_2$, consequently, result in two discrete energy states. While without an external magnetic field, the states are energetically equal, energy differences arise in the presence of an external magnetic field caused by the Zeeman effect.

Nuclear resonance phenomena are based on the excitation of nuclear spin transitions between different m_I. The required energy ΔE is proportional to the strength of the external magnetic field B_0 and to the magnetogyric ratio γ of the considered atomic nuclei

$$\Delta E = \gamma \hbar B_0 = \hbar \omega_L \tag{1}$$

This energy is irradiated as resonant electromagnetic waves with the resonance frequency ω_L, which is called Larmor frequency. The resonant frequencies are influenced by individual small magnetic fields, which are generated by the influence of the electronic environment around an atomic nucleus or by interaction with adjacent atomic nuclei in the same molecule. This leads to slightly different resonance frequencies ω_L of atoms in different positions in a molecule. A descriptive, more comprehensive, and detailed explanation of general magnetic resonance principles can be found elsewhere.[17,34]

The slightly varying Larmor resonance frequencies ω_L of different atoms in a molecule lead to different resonance lines in the resulting NMR measurements. Since all molecules of a given chemical component have essentially the same structure, these different resonance lines add up and can be detected as separated signals and signal groups in the resulting NMR spectrum. They are normally indicated by relative frequency differences between a signal of certain nuclei in the investigated molecule (ν_{sample}) and those of a nucleus in a standard (ν_{ref}). These differences are assigned as chemical shifts δ, whereas the reference is assigned to a chemical shift of zero. The chemical shifts δ are calculated according to

https://dx.doi.org/10.1021/acsomega.0c02059
ACS Omega XXXX, XXX, XXX−XXX

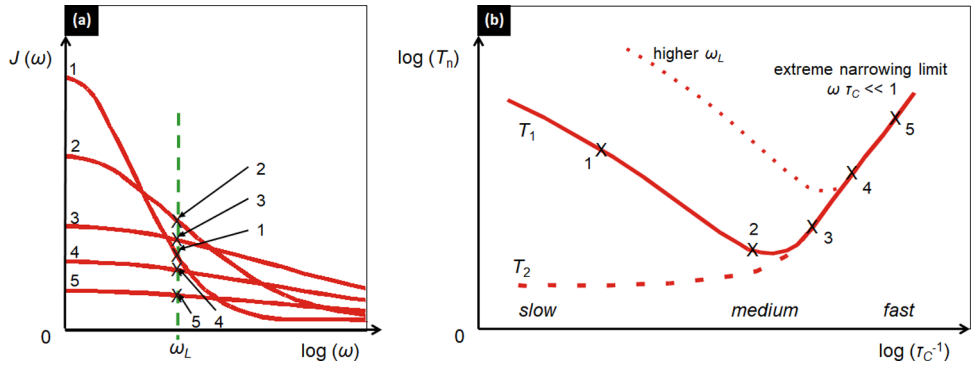

Figure 1. (a) Schematic representation of the spectral density at different temperatures: 1 (low) to 5 (high). For a selected Larmor frequency ω_L, the relative amount of spins possessing this particular frequency is displayed (green dashed line). (b) Schematic plot of number of spins vs molecular tumbling rate (τ_C^{-1}) for T_1 times (solid line). At lower temperature, T_2 times differ from T_1 times due to changes in molecular interaction (e.g., tendency to form aggregates). Hence, T_2 times have a different behavior, which is shown with a dashed line. The change in the behavior of T_1 times, based on different B_0, is illustrated by a dotted line. The temperature range in which NMR spectra are recorded, which are used for the determination of molecular structures, is at relatively high temperatures in the "extreme narrowing limit", where $\omega\tau_C \ll 1$ leading to signals with small line width at half-height.

$$\delta = (\nu_{sample} - \nu_{ref})\ 10^6/\nu_{ref} \quad (2)$$

They are hence independent of the spectrometer magnetic field strength B_0 and given in parts per million (ppm) in order to allow assignment and identification of the nuclei using the chemical shift (δ). This powerful tool of varying chemical shifts is most commonly used for structure determination and can also provide information about the interaction between two (different) molecules.

Apart from chemical shift δ, two further observables are primarily investigated in the present research, namely, T_1 and T_2 relaxation times. The T_1 relaxation is understood in NMR spectroscopy and MRI to be a process that causes nuclear spin magnetization to return to its equilibrium state after excitation. The T_2 relaxation takes place through the desynchronization of the spins within the coherence plane. These effects are based on two relaxation mechanisms, which are described by the relaxation times T_1 and T_2 and are caused by different magnetization components. The T_1 time is derived from the recovery of the full magnitude into the direction M_z according to the Bloch equations.[35] It is called spin−lattice relaxation time as the absorbed energy is redistributed to the thermal bath providing a measure of the enthalpy of the system. The recovery follows exponential behavior described by

$$\frac{dM_z}{dt} = \frac{(M_0 - M_z)}{T_1} \quad (3)$$

The T_2 time describes the disappearance of the transverse magnetization M_x and M_y according to the Bloch equations.[35] Within this process appears the loss of phase coherence between spatial neighboring spins, which for hydrogen carrying liquids and solution includes not only intramolecular modes but also local intermolecular modes. T_2 is named spin−spin relaxation time as it is an adiabatic process whereby energy is redistributed locally but without the whole spin system losing energy. This provides a representation of the local entropy of the spin system. The recovery follows exponential behavior described by

$$\frac{dM_x}{dt} = \frac{-M_x}{T_2} \quad (4)$$

$$\frac{dM_y}{dt} = \frac{-M_y}{T_2} \quad (5)$$

The subatomic origin of the relaxation processes is the interaction between the excited spins and their environment, in particular with a magnetic gradient field induced by molecular motions of surrounding other spins. These spins, e.g., from other nuclei or unpaired electrons, cause an additional local magnetic field that oscillates in time through Brownian motion and the rotation of the molecules. The most important interaction mechanism for the nuclei with $I = {}^1/_2$ is the magnetic dipole−dipole interaction. Spectral components at the resonance frequency allow transitions and thus lead to the relaxation of the previously excited nuclei. In the case of a Brownian motion of the molecules, the resulting time-independent autocorrelation function can be set by an exponential decay with the correlation time τ_C. The solution of the Fourier transformation of this function is called spectral density function $J(\omega)$

$$J(\omega) = \frac{2\tau_C}{1 + \omega^2\tau_C^2} \quad (6)$$

This equation represents the distribution of nuclei possessing different correlation times τ_C. Figure 1a shows the schematic function for five different molecular mobilities, triggered for example by different sample temperatures. It should be noted that at a given frequency corresponding to the Larmor frequency ω_L, there is a temperature at which a maximal number of nuclei have this frequency.

In Figure 1b, the number of respective nuclei with Larmor frequency ω_L is plotted against the molecular tumbling rate (reciprocal of the correlation time τ_C). For the T_1 time, an extremum is easily detectable, in which the relaxation time has a minimum (solid line). The position of this extremum depends on the Larmor frequency ω_L and thus on the applied external magnetic field B_0. The dotted line shows the course for a larger B_0 and a consequently higher ω_L. This is to be considered within investigations of the temperature dependence of T_1 relaxation times at different magnetic field strengths B_0 in NMR and MRI. The T_2 time shows a different behavior at lower temperatures and tumbling rates (dashed line). Molecular interactions, such as aggregate formation, strongly

https://dx.doi.org/10.1021/acsomega.0c02059
ACS Omega XXXX, XXX, XXX−XXX

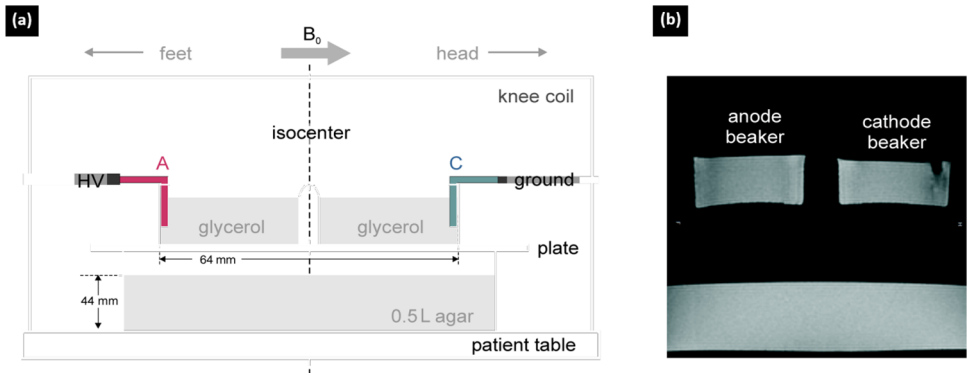

Figure 2. Diagram of the experimental setup used for the presented study. (a) Experimental setup and (b) central sagittal slice used in this study.

favor transitions in transverse magnetization (M_x and M_y), resulting in faster T_2 relaxation and thus shorter T_2 times. Further detailed explanations of chemical shifts and relaxation phenomena can be found elsewhere.[17,34]

3. MATERIALS AND METHODS

3.1. MRI Imaging of Glycerol Electrohydrodynamic Bridges in the Magnetic Field Environment. *3.1.1. Sample Preparation.* Electrohydrodynamic bridges in glycerol were prepared in a manner consistent with the method described previously for studies in water[36] using nonmagnetic materials in the construction of the fixating armature, cable supports, and electrode mounts. The glass beaker diameter was 30 mm, and the beaker spouts were left in contact throughout the measurements for higher stability and to avoid bridge rupture, liquid leakage, and electrical arcing in the setup − all of which could pose a hazard to the MRI scanner. Such a bridge extended over 4 mm from the anode side to the cathode side beaker but was always supported by glass. These types of bridges behave in a manner consistent with horizontal aqueous EHD bridges (see the characteristic of EHD bridges[8]).

MRI of the glycerol bridges was performed on a 1.5 T scanner at a resonance radio frequency (RF, Larmor frequency) of 63.70 MHz (Magnetom Sonata, Siemens Healthcare, Erlangen, Germany) using a standard circular-polarized knee coil. The experimental setup is illustrated in Figure 2. The glycerol bridge was aligned so that the long axis of the bridge was parallel to the main magnetic field B_0 with the anode placed toward the foot end of the patient table and the cathode toward the head end. The bridge center was located in the isocenter in the head−feet direction, in the right−left direction, and some millimeters above the isocenter in the anterior−posterior direction.

A plastic box filled with 500 mL of agar and covered with a glass plate formed the electrically insulating support base for the beakers. The agar phantom was used as a signal reference for intensity normalization. All materials were fixed in place using MR compatible tape, which does not produce artifacts in the recorded images. Platinum foil (99.999% Pt, MaTeck GmbH, Jülich, Germany) was soldered to both the HV and ground leads with wires that are sufficiently long (∼10 m) to reach from the experiment at the MR scanner isocenter to the power supply located just outside the room via an RF suppressing pass-through in the Faraday cage wall.

3.1.2. T_1 and T_2 Relaxation Time Measurements. The bridges studied for this section were prepared from anhydrous glycerol (49767-100ML, Lot # BCBK7056V, Sigma Life Science, St. Louis, MO, USA). A total of 31 pairs of T_1 and T_2 time measurements were made using data collected from nine glycerol bridges operated at 16 kV and 10−20 μA. Five regions-of-interest (ROIs) in the glycerol bridge were chosen for determination of magnetic relaxation times, with ROI 5 recording the bridge section, ROIs 3 and 4 the spout sections, and ROIs 1 and 2 the beaker sections, all shown in Figure 3.

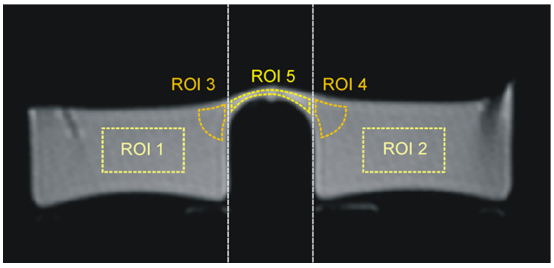

Figure 3. Segmentation of five regions-of-interest (ROIs) in the glycerol bridge for determination of magnetic relaxation times. ROI 1, anode beaker; ROI 2, cathode beaker; ROI 3, spout of anode beaker; ROI 4, spout of cathode beaker; ROI 5, bridge section.

Glycerol temperature was measured before and after bridge operation in both the anode and cathode beaker with an alcohol thermometer. The typical temperature rise in the beakers during two complete measurement series (requiring ∼1 h) was 1.5 ± 0.5 °C.

Thermographic recordings done in a separate study[8] with glycerol bridges operated at 0.3 W clearly show that the glycerol warms during bridge operation. Since the EHD bridge acts as an Ohmic resistor, most of the heating is localized to the bridge itself. Because temperature monitoring inside was not feasible inside the MR coil, temperatures were estimated outside the MRI scanner and without air cooling usually present in the test section of MRI scanners. Direct probe measurements were performed using fiber optic temperature probes (OTG-Q, Opsens, Québec, Canada).

Before applying HV to the glycerol setup, an isotropic three-dimensional spoiled fast low-angle shot (FLASH) sequence covering the experimental setup was employed to optimize and fix the sagittal imaging plane visualizing beakers and the glycerol bridge. Estimation of relaxation times in these regions was based on two-dimensional spin echo measurements in this plane. For T_1 estimation, spin echo sequences with two different repetition times (T_R) were acquired with the following protocol parameters: T_R, 70 and 300 ms; echo time (T_E), 8 ms; bandwidth, 170 Hz/pixel; field-of-view, 150 ×

https://dx.doi.org/10.1021/acsomega.0c02059
ACS Omega XXXX, XXX, XXX−XXX

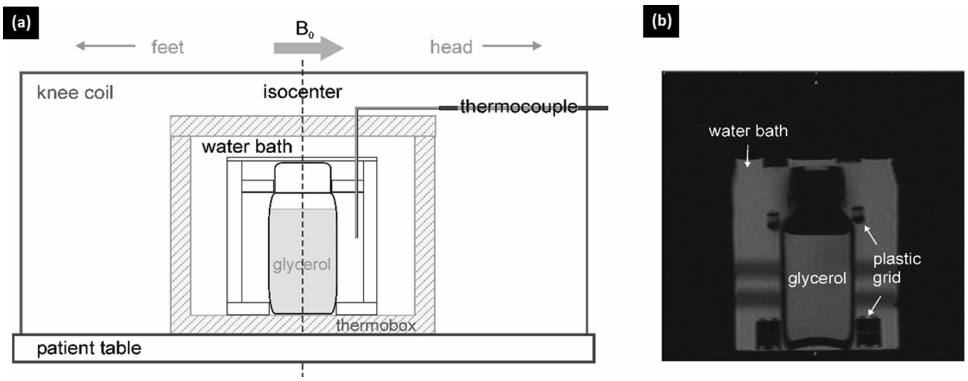

Figure 4. Experimental setup for the calibration of temperature behavior of relaxation times of glycerol. (a) Experimental setup and (b) central sagittal slice used in this measurement.

150 mm^2; resolution, 0.8 × 0.8 × 3.0 mm^3; number of averages, 1; imaging time, 17 s / 1 min 01 s, for the two repetition times.

For T_2 estimation, a multiecho spin echo sequence with 16 different echo times (8.3/16.6/24.9/33.2/41.5/49.8/58.1/66.4/74.7/83.0/91.3/99.6/107.9/116.2/124.5/132.8 ms) was used. Further protocol parameters were as follows: T_R, 400 ms; bandwidth, 280 Hz/pixel; field-of-view, 150 × 150 mm^2; resolution, 0.8 × 0.8 × 3.0 mm^3; number of averages, 3; imaging time, 3 min 54 s. To compensate for a decreased signal-to-noise ratio in the images during the existence of the bridge, measurements for T_1 determination were three-fold averaged and measurements for T_2 determination six-fold, with correspondingly longer imaging times.

For each pair of spin echo images (with different T_R times) and each multiecho spin echo measurement, average relaxation times were estimated in five ROIs in both beakers, near the spouts or bridge base, and in the bridge itself (Figure 3). In both spin echo images with different T_R, mean ROI signal intensities were derived from ROIs drawn as similar as possible but carefully excluding electronic noise artifacts and partial volume areas in the time-varying bridge. Mean T_1 times at the five localizations were determined from fitting the mean signal intensities of corresponding ROI pairs to the spin echo signal intensity equation[38]

$$\text{signal intensity} = A\left(1 - 2e^{-\left(T_R - \frac{T_E}{2}\right)/T_1} + e^{-T_R/T_1}\right) \quad (7)$$

where A and (mean) T_1 are the fitting constants. Fitting was performed using the statistical analysis software package NCSS.[37] For T_2 estimation, the image with the lowest echo time (T_E = 8.3 ms) and images with predominant noise contribution (typically T_E > 83 ms) were excluded from the series of multiecho spin echo images. Pixel signal intensities of the remaining multiecho spin echo images were linearly fitted to the logarithm of the signal intensity equation[38]

$$\text{signal intensity} = Ae^{-T_E/T_2} \quad (8)$$

to determine T_2 of the pixel (and an additional fitting constant A). This calculation was performed for any pixel by the scanner software (syngo VA25, Siemens Healthcare, Erlangen, Germany) to produce a T_2-map. Mean T_2 values in both beakers, at both beakers' spouts, and in the bridge were determined from corresponding ROIs.

3.1.3. Temperature Calibration Measurements. In order to perform relaxation-based thermometry, a calibration standard was imaged and processed using the same methods as described for the bridge. The temperature calibration sample was a bottle of glycerol immersed in a water bath held in an insulating box. The measurements were performed twice, once with an open bottle of glycerol and once with a sealed bottle of anhydrous glycerol. A thermocouple recorded the temperature of the sample, which was allowed to equilibrate between temperature steps. A diagram of the setup is shown in Figure 4.

3.1.4. Single-Voxel Spectroscopy in the MRI Scanner. For the recording of single-voxel proton spectra in the MRI, a tube (1 cm diameter) filled with glycerol was equipped with a cathode and anode. Parameters of the employed STEAM (stimulated echo acquisition method) sequence were as follows: T_R, 1300 ms; T_E, 20 ms; mixing time (T_M), 10 ms; voxel size, 10 × 10 × 25 mm^3; number of averages, 350; imaging time, 7 min 35 s. The measurements were taken from a region between the electrodes. Spectra were recorded without electrical voltage and under a voltage of 3.5 kV. The RF was fixed to the resonance frequency of the proton in H_2O. Processing of the spectra was performed by the standard scanner software.

3.2. High-Field Nuclear Magnetic Resonance Spectroscopy of Glycerol. *3.2.1. Sample Preparation.* To obtain a sample for high-field NMR measurement, glycerol has been used, without an electric field applied to the sample. The amount of water from humidity was in the same range as in the glycerol used for the MRI measurements. The glycerol was filled into 5 mm high-precision NMR sample tubes (Wilmad 507 PP 8″, Armar AG, Dottingen, Switzerland). A C_6D_6 vortex capillary was added to the probes to avoid mixtures between the deuterated substance used for the lock and the investigated liquids. Comparable systems have been described earlier.[39,40]

3.2.2. Nuclear Magnetic Resonance Spectroscopy. All spectra were recorded on a DRX-400 AVANCE spectrometer (Bruker, Rheinstetten, Germany) with a two channel z-gradient inverse probe head using the bundled software Topspin 1.3 (Bruker, Rheinstetten, Germany). Irradiation and measurement frequency in a field strength of 9.4 T was 400.13 MHz for protons (^1H). Temperature was adjusted in the range between 27 and 55 °C with an accuracy of ±0.05 °C. The NMR tube was rotated during the measurements with 20 rps. For all measurements, the residual C_6D_5H in not fully deuterated C_6D_6 in the vortex capillary was used as external reference (δ_H = 7.15 ppm).[41]

One-dimensional proton (^1H) spectra were recorded with a ^1H-pulse flip angle of 30°, acquisition of 64k data points, and a relaxation delay of 1.0 s. Free induction decays (FID) of eight

https://dx.doi.org/10.1021/acsomega.0c02059
ACS Omega XXXX, XXX, XXX−XXX

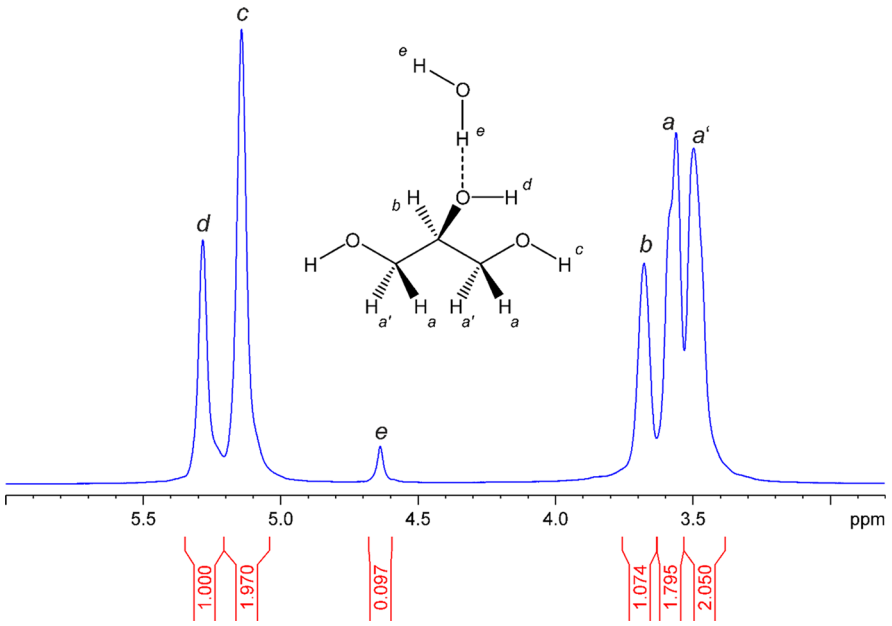

Figure 5. ^{1}H NMR spectrum of glycerol at 27 °C with peak assignments as indicated in the molecular structure. The integrals give the relative abundance of the protons. Water content can thus be determined to be about 5% (mol/mol), which corresponds to about 1% (w/w). The numbers underneath the plot provide the integral values for each signal group.

scans were added for one spectrum. The summed FID was directly Fourier transformed to gain spectra with a spectral range of 8000 Hz.

T_1 time constants for different groups of protons were determined by the inversion recovery method changing the recovery delays in 12 steps from 10.0 ms to 8.0 s (0.01/0.1/0.2/0.3/0.5/0.7/1.0/1.5/2.0/3.0/4.0/8.0 s).[42] For each scan, a 180° pulse, the recovery delay, and a 90° pulse were followed by the acquisition. During acquisition, 32k data points were collected and the subsequent relaxation delay took 5.0 s. FIDs resulting from eight scans were added prior to Fourier transformation, which led to spectra with a spectral range of 6000 Hz. Signal intensity was determined by integration. The T_1 times were calculated using the software Topspin 4.0.5 (Bruker, Rheinstetten, Germany).

The T_2 time constants for different groups of protons were measured with the spin echo sequence (CPMG) using a τ of 10.0 ms and varying the number of spin echo blocks (2τ-times) from 2 to 50[43,44] in 12 steps resulting in times of 0.04/0.08/0.16/0.24/0.4/0.8/1.4/2.2/3.2/4.4/6.0/10.0 s. For each scan, a 90° pulse was followed by the series of spin echo blocks (τ - 180° pulse - τ) prior to the acquisition. During acquisition, 32k data points were collected and the subsequent relaxation delay took 5.0 s. FIDs resulting from eight scans were added prior to Fourier transformation, which led to the spectra with a spectral range of 6000 Hz. Signal intensity was determined by integration. The T_2 times were determined manually using the software Topspin 4.0.5 (Bruker, Rheinstetten, Germany) and considering the intrinsic line over the signal intensity with respect to intensity change caused by scalar ^{1}H−^{1}H coupling during the delay times.

4. RESULTS AND DISCUSSION

4.1. Nuclear Magnetic Resonance Spectroscopy. For a better understanding of the data recorded by MRI, ^{1}H NMR spectra as well as T_1 and T_2 times of glycerol were sampled in the NMR spectrometer at 9.4 T without an electric field applied to the liquid.

The proton (^{1}H) NMR spectrum of anhydrous glycerol is shown in Figure 5 for a temperature of 27 °C and a Larmor frequency of 400 MHz. Three groups of resonance peaks with six peaks altogether caused by the 10 protons in glycerol and water are clearly identifiable in Figure 5. In detail, a multiplet of partly overlapping signals from the carbon bound protons (δ_H = 3.68 (CH); δ_H = 3.55 (CH_2 {2 × a}); δ_H = 3.48 (CH_2 {2 × a'})), two singlets from the alcohol protons (δ_H = 5.30 ppm (secondary alcohol) and δ_H = 5.15 ppm (two primary alcohols)), and weak contribution by hydration water (δ_H = 4.63 ppm) are visible in Figure 5. The latter mentioned signal is caused by a small amount of water, which is always present in glycerol due to its hygroscopicity and sample preparation in open air − a situation comparable to the open-air measurements in the MRI.

The line widths at half-height of all signals are in the range of ca. 5−10 Hz. This is quite large compared to standard ^{1}H NMR measurements showing line widths at half-height in the range of ca. 1−2 Hz. Such broad lines are caused by relatively fast nuclear spin relaxation.[45,46] Rather slow chemical exchange of the free protons furthermore causes the separation of the proton signals of the two different types of hydroxyl groups and water. With rising temperature, the molecular movement and chemical exchange are enhanced. These effects cause narrowing of the line width at half-height for proton signals due to increasing relaxation times. However, concomitant faster chemical exchange of the oxygen-bound protons (R−OH and H_2O) leads to coalescence of their signals. Hence, for alcohols and water, the three signals merge toward one broad signal with increasing temperature, whereas the fine splitting of the carbon-bound protons becomes more pronounced (data not shown). However, within the investigated temperature range, all protons lead to separated signals, which allow individual determination of T_1 and T_2 times for all nuclei in nearly all measurements.[17,34]

https://dx.doi.org/10.1021/acsomega.0c02059
ACS Omega XXXX, XXX, XXX−XXX

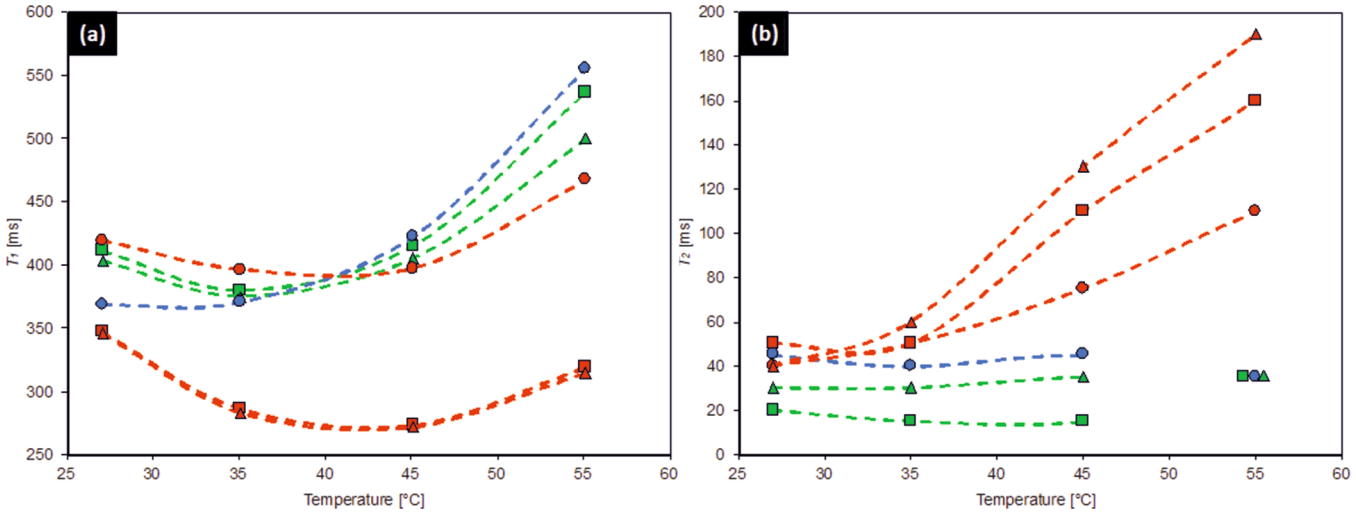

Figure 6. Effect of temperature on relaxation times for the six different groups of protons in glycerol and water, which are indicated in Figure 5. The T_1 times and T_2 times are shown in panels (a) and (b), respectively. Relaxation times of carbon-bound protons are indicated in red (red circle: CH; red square: CH_2; red triangle: CH_2). T_1 and T_2 times of the alcohol protons are indicated in green (green triangle: primary alcohol; green square: secondary alcohol), and those of protons from water are indicated with blue circles. At 55 °C, the three signals of protons in alcohol and water overlap due to coalescence caused by faster chemical exchange. For T_1 times, separate determination was possible, while for the T_2 time, only an averaged value was determined. The standard deviation for all measurements presented in Figure 6 is on the order of 10^{-2} to 10^{-3} ms.

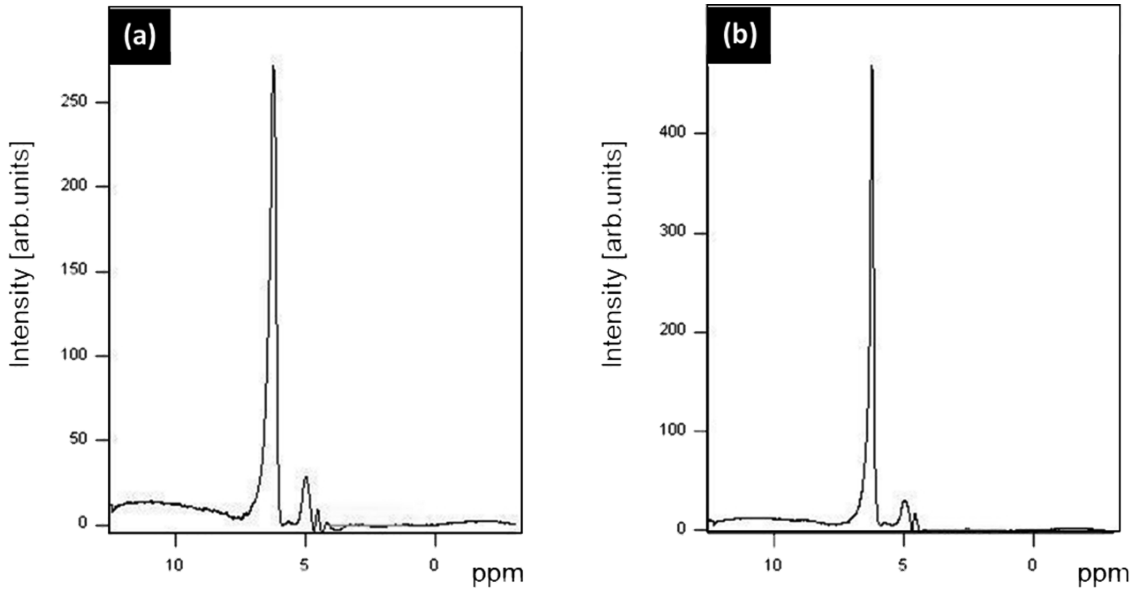

Figure 7. ^{1}H single-voxel spectroscopy measurements of glycerol recorded in the MRI scanner. Panel (a) shows the measurement at 0.0 kV, while panel (b) shows the measurement at 3.5 kV.

Values of T_1 and T_2 relaxation times in glycerol at varying temperatures (27 to 55 °C) separated for each of the six signals indicated in Figure 5 are plotted in Figure 6. T_1 times of the protons in OH groups and water increase with temperature (Figure 6a). This behavior indicates that the molecular motion of these temporarily dissociated protons leads to correlation times, which tend to a branch known as the extreme narrowing limit, which appears on the right side in Figure 6a. In contrast, all carbon-bound protons, which are indicated in red in Figure 6a, show minimum T_1 times at about 42 °C. This extremum indicates that these molecular moieties have a maximal relaxation for the 400 MHz Larmor frequency used.[47] This is in reasonably good agreement with results from Noack and Preissing for averaged T_1 times of all protons in entire glycerol.[45] The temperature-dependent change averaged over T_1 times of all protons in glycerol and water is furthermore in agreement with those determined in the MRI at lower Larmor frequency for the same temperature range (see below).

The T_2 times of the protons in glycerol (Figure 6b) show slightly different effects on temperature changes compared to the T_1 times. The carbon-bound protons show increasing T_2 times with rising temperature, which fits well to the temperature-dependent spin−spin relaxation of entire glycerol.[45] In contrast, T_2 times of the protons in OH groups and water change only slightly in the investigated temperature range, although coalescence and concomitant increasing T_1 times indicate changes in their tumbling rates. However, T_2 times of all these protons are rather small in the measured temperature range. This indicates that they make a major contribution to spin−spin relaxation of entire glycerol. Possible

https://dx.doi.org/10.1021/acsomega.0c02059
ACS Omega XXXX, XXX, XXX−XXX

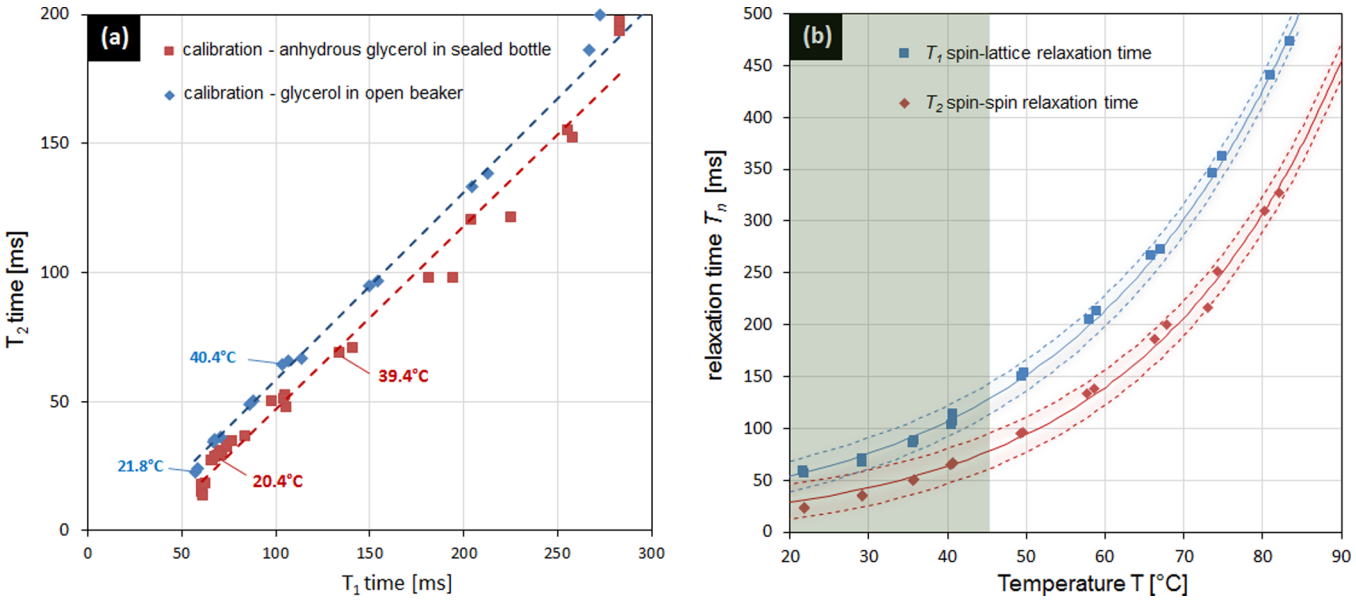

Figure 8. (a) Linear regressions of T_2 on T_1 relaxation times for different temperatures ranging from 22 to 83 °C performed in a sealed bottle of anhydrous glycerol (red squares and dotted line) and in an open beaker filled with glycerol (blue diamonds and dotted line). All data were recorded with MRI without HV applied to the sample. Panel (b) provides the temperature calibration curves with glycerol open to the atmosphere recorded for T_1 and T_2. The fit uses a robust Leveberg−Marquardt nonlinear least squares fit; 99% confidence bounds are shown as dashed lines. The shaded area indicates the temperature range of the EHD bridge during operation (app. 50 to 120 ms for T_1).

temperature-dependent changes in these T_2 times are only moderate, indicating relatively small variations in their tumbling rate. However, measurement of these temperature dependent changes is not very accurate due to the signal broadening caused by coalescence. Thus, it is not possible to make a precise statement about relatively small changes in the T_2 times in this temperature and relaxation time interval.

4.2. Single-Voxel Spectroscopy in an Electric Field. Since the EHD setup was too large to be placed in a high-field NMR spectrometer at 9.4 T, ^{1}H NMR spectroscopic measurements of glycerol were performed in the 1.5 T MRI scanner using the stimulated echo acquisition mode sequence (STEAM).[48,49] A spectrum recorded without electrical HV is shown in Figure 7a. Here, all signals are shifted about 1.5 ppm compared to those in the ^{1}H NMR measurement discussed in the previous section (Figure 5), which is caused by referencing to different standards (eq 2). The signals of protons from OH groups and H_2O can be seen at app. 6.5 ppm, and signals from alkyl protons are at app. 5.0 ppm. Due to the comparatively poor spectral resolution compared to the NMR measurements, the signals of these two signal groups each overlap and thus both coincide into undissolved signal groups. In contrast to the signal intensities of the NMR measurement (Figure 5), in the MRI measurement, the signals of protons from OH groups and H_2O have a much larger signal intensity than signals from alkyl protons.

These differences in signal intensity between ^{1}H NMR spectra recorded in NMR and single-voxel spectroscopy in MRI are very likely caused by three different reasons: On the one hand, the relaxation times of the nuclei are significantly different, as can be seen in Figure 6. Within T_M and T_E of the STEAM sequence, this leads to a differently rapid reduction in signal intensity of the two signal groups. Furthermore, there is a development of homonuclear coupling between the alkyl protons during these times. This leads to the formation of signal forms with dispersion components in the signal group of the alkyl protons. Due to the low digital resolution, the resulting signal shape is not exactly represented and consequently leads to a significantly reduced intensity of the signal group. This effect is explained and discussed in detail elsewhere.[49] A third reason can be a low amplitude and limited bandwidth of the RF in the MRI scanner, by which the two signal groups are stimulated to different degrees. This would be comparable to selective excitation in high-field proton NMR measurements in principle. A close examination of which of these three effects is responsible to which extent for the different intensities of the two signal groups in the single-voxel spectroscopy in the 1.5 T MRI scanner has not been carried out.

The spectrum shown in Figure 7b presents the single-voxel ^{1}H spectrum under a voltage of 3.5 kV. Interestingly, the chemical shifts of all protons do not significantly differ between the two measurements with and without HV excitation of glycerol. Hence, for the discussion in the next sections, it can be stated that any influence on the chemical shift from the HV electric field applied to the glycerol bridge setup (Figures 2 and 3) can be neglected. This is correct both for frequency differences between the signal groups as well as between the signal groups and the Larmor frequency. Comparing Figure 7a,b, it is interesting to note that the signals of the protons from OH groups and H_2O at about 6.5 ppm increase in amplitude and decrease in line width, although no unambiguous interpretation for that can be given from this measurement.

Comparing the spectra recorded by NMR (Figure 5) and MRI (Figure 7), some general conclusions can be drawn concerning the use of MRI. On the one hand, in MRI, the relaxation times are averaged over all proton signals in the entire frequency region. This is due to the fact that only a simultaneous excitation of the entire frequency range as well as a summed recording over all excited frequencies is possible. The varying proportion of signal intensity over all these proton

https://dx.doi.org/10.1021/acsomega.0c02059
ACS Omega XXXX, XXX, XXX−XXX

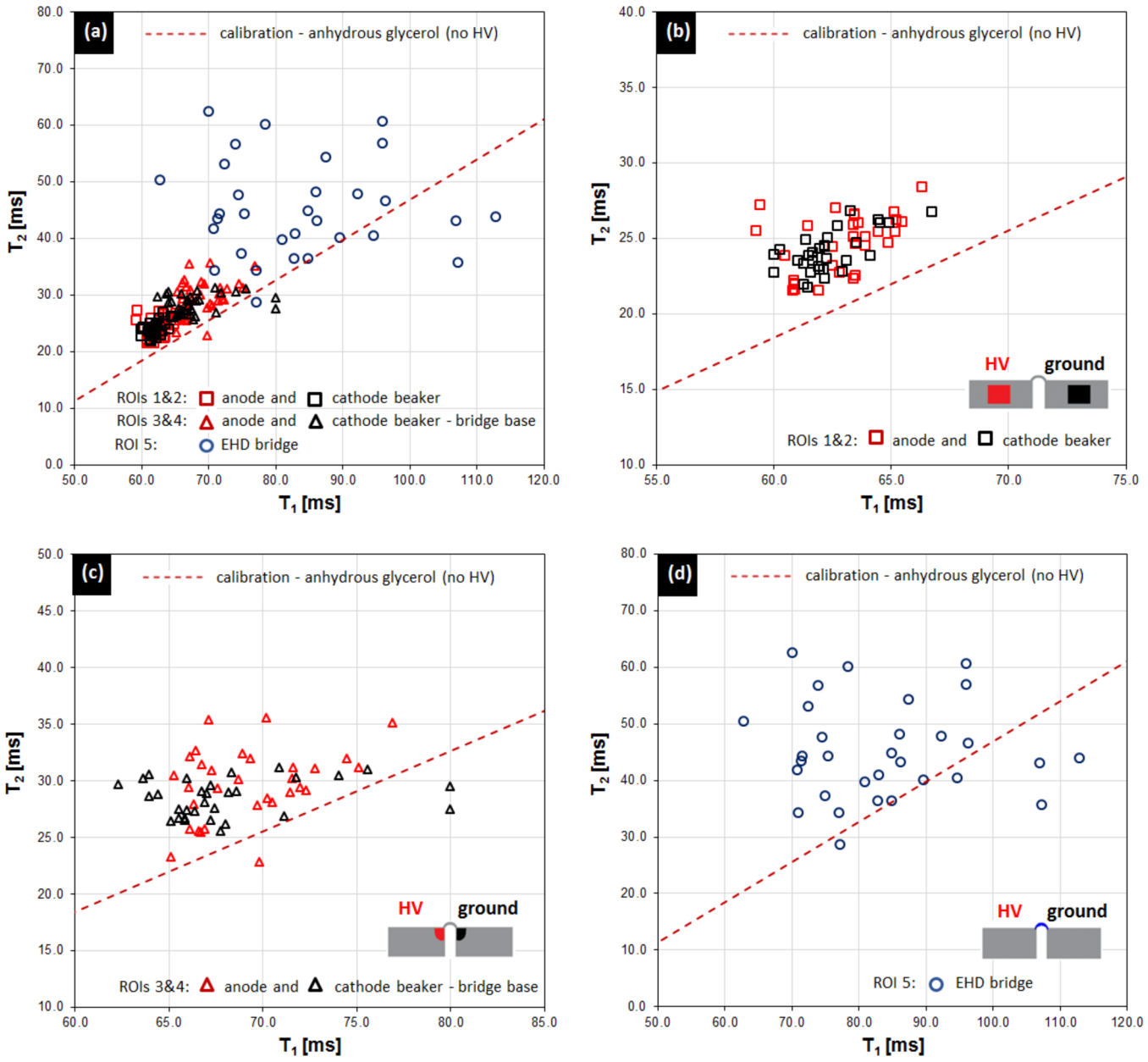

Figure 9. Comparison of T_2 on T_1 relaxation times taken from nine glycerol bridges. Relaxation times were extracted from five regions-of-interest (see Figure 3): (a) bulk anolyte (ROI 1 red squares), bulk catholyte (ROI 2 black squares), anode bridge base (ROI 3 red triangles), cathode bridge base (ROI 4 black triangles), and the bridge itself (ROI 5 black circles). Red indicates those data from the high-voltage (HV) beaker. Panel (a) plots the full dataset; panels (b–d) show the datasets for bulk, bridge base, and bridge, respectively. The glycerol EHD bridges were operated at 16 kV and 10–20 μA.

signals leads to contributions from different protons, which are not equivalent to their molar ratio in the molecule. Therefore, the proportion of OH protons and H_2O protons (signal at app. 6.5 ppm) is several times larger than that of the alkyl-bound protons (signal at app. 5.0 ppm) in the MRI spectra.

For determination of T_1 times, this effect is less critical in the temperature range above 42 °C as their temperature dependence tends to be similar for all protons (Figure 6a). This is in particular correct for the measurements at 1.5 T as the extremum of the spectral density is shifted to lower tumbling rates (smaller τ_C^{-1}) than measurements at 9.4 T (see Figure 1b).

In the temperature-dependent changes of the T_2 times, however, in MRI, the over-represented T_2 times of the OH and H_2O protons show only small changes in the double-digit millisecond range (15–70 ms), while the contribution of the increasing T_2 times of alkyl protons with rising temperature is under-represented (compare Figure 6b). The difference cannot be exactly determined or corrected from the relative signal integrals in the spectra shown in Figure 7 as the chemical shift of the OH proton and H_2O proton signal itself is slightly temperature-dependent.

These results reveal that averaged T_1 relaxation times of glycerol recorded in an MRI scanner will tend to provide a reasonably accurate estimation of temperature as all nuclei behave in the same way in this temperature range. It has, however, to be noted that in MRI for T_2 time measurements, the relatively constant contribution of the OH protons is over-

https://dx.doi.org/10.1021/acsomega.0c02059
ACS Omega XXXX, XXX, XXX−XXX

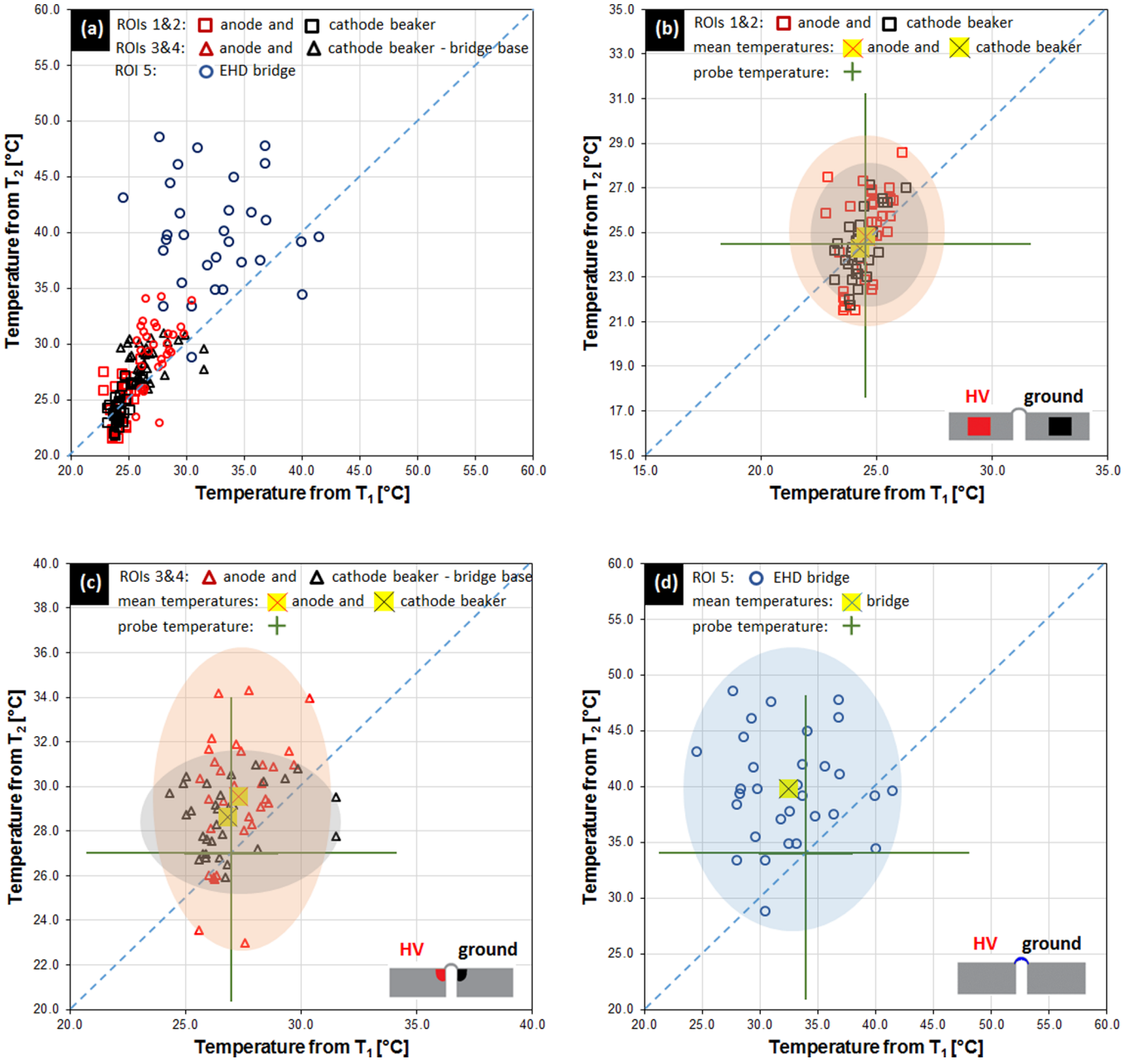

Figure 10. Comparison of relaxation-derived temperatures taken from nine glycerol bridges. The fitted temperatures derived from T_1 and T_2 are plotted against each other. Relaxation-derived temperatures were extracted from five regions-of-interest (see Figure 3): bulk anolyte (ROI 1 red squares), bulk catholyte (ROI 2 black squares), anode bridge base (ROI 3 red triangles), cathode bridge base (ROI 4 black triangles), and the bridge itself (ROI 5 black circles). Red indicates those data from the high-voltage (HV) beaker. For reference, probe temperatures are marked with a cross. All of the investigated ROIs are plotted in panel (a), whereas similar regions are compared in (b) the center of the beakers, (c) near the bridge base, and (d) for the bridge section.

represented in the averaged T_2 time, while the more temperature-dependent portion of the alkyl protons is significantly under-represented due to their smaller contribution caused by a lower signal intensity. For further discussion, it is important to note that this is true for measurements with and without HV excitation.

4.3. Temperature Calibration of Relaxation Times of Glycerol by Magnetic Resonance Imaging. Within the temperature ranges of the calibration experiments of 22 to 83 °C, T_1 and T_2 relaxation times demonstrated an almost linear relationship (determination coefficient R^2 = 0.9955 for the open and R^2 = 0.9813 for the closed bottle, respectively). Figure 8a represents the T_2 versus T_1 relaxation time plots together with the linear regressions.

The temperature calibration measurement data for T_1 and T_2 were fitted using a type of exponential function as given in

$$T_{1,2} = ae^{(b(T-c))} \quad (9)$$

The fit coefficients a, b, and c were derived using a nonlinear regression in the statistical analysis software package NCSS.[37] Figure 8b demonstrates the T_1 and T_2 time temperature calibration curves of the experiment with glycerol open to the atmosphere with R^2 values of 0.9988 and 0.9952 for T_1 and T_2, respectively.

https://dx.doi.org/10.1021/acsomega.0c02059
ACS Omega XXXX, XXX, XXX−XXX

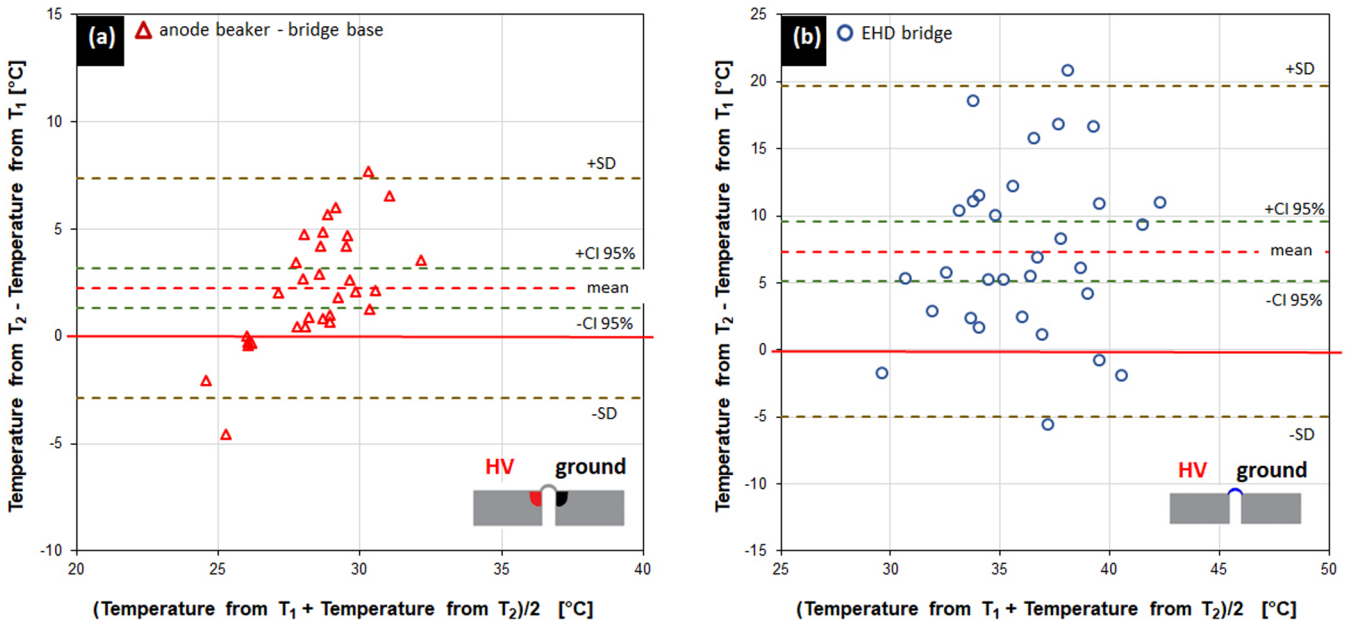

Figure 11. Bland–Altman plot for the temperature recordings obtained from T_1 and T_2 times recorded by MRI in order to show the significance of the temperature shifts recorded by the T_2 times when a mild HV is applied to glycerol in the anode bridge base (a) and the EHD bridge (b). Plotted are the mean values, the standard deviations (SD), and the 0.95 confidence interval of the mean (CI 95%), as well as the zero line.

4.4. Magnetic Relaxation Mapping in Electrically Stressed Glycerol. Results of 31 paired T_1 and T_2 relaxation time measurements collected from nine EHD glycerol bridge experiments are shown in Figure 9. While Figure 9a plots show the results of all five evaluated ROIs, Figure 9b–d shows the datasets for bulk, bridge base, and bridge, respectively.

In the beakers (ROI 1 and ROI 2, Figure 9b), the determined values for the relaxation times have a relatively low spread and the entropy-related spin–spin relaxation time T_2 does follow the temperature rise in relation to the T_1 time approximately the same way it does in the bulk without an HV applied (R^2 = 0.2137 for ROI 1 and R^2 = 0.4101 for ROI 2). Since the EHD bridge acts as an Ohmic resistor, a main voltage drop of 16 kV applies to the short section between the onset of the bridge in the anode beaker (ROI 3) and the onset of the bridge in the cathode beaker (ROI 4) and not to the bulk in the beakers (compared also to aqueous EHD bridges[7]). The heating of the liquid in the beakers is mainly due to transport of the material from this bridge section. For this reason, the temperature in the beakers is about room temperature or slightly above (app. 25 °C with T_1 at 60 to 65 ms according to the calibration characteristic plotted in Figure 8b).

The spread in data is much larger in ROIs 3 and 4, where the bridge base forms in the anode and the cathode beakers (Figure 9c). Probe measurements revealed an average temperature rise of app. 8 °C, a little higher at the anode side, compared to the cathode side of the bridge (see Figure 3, 25–30 °C, T_1 app. 70 ms). When the temperature in these sections increases, the T_2 time no longer follows accordingly while the HV is applied to the liquid (R^2 = 0.1225 for ROI 3 and R^2 = 0.0364 for ROI 4).

The most pronounced spread can be found in the ROI 5 with an average temperature rise by 15 °C (35 °C, T_1 app. 80–85 ms). From the bridge section, the highest variations in relaxation time are reported; in this ROI, measurement artifacts are likely the cause. Even at low speed, fluid flow can transport signal out of the measurement volume and temperature fluctuations during measurement times will introduce nonlinearities in the relaxation dynamics, causing the strong variations in recording T_1 and T_2 times. However, similar to the cathode beaker's bridge base, in average, there is nearly no change of T_2 observed in the bridge section (R^2 = 0.0021) for a broad range of T_1 times (between 60 and 120 ms, or 25 to 40 °C according to the calibration curves in Figure 8b).

In Figure 10, the same data are given as temperatures, with the temperatures derived from the calibrated relaxation times (T_1 as well as T_2) for glycerol as shown in Figure 8b for the open beaker configuration without HV applied.

From the calibration curves plotted in Figure 8b, it is evident that in the temperature range discussed (shaded area in Figure 8b), the possibility to estimate temperatures by MRI is limited due to the low dependence of relaxation times on temperature and the large uncertainties in this temperature range. On the other hand, from Figure 9 and another publication,[7] we learn that the glycerol in the beakers (ROIs 1 and 2) is not exposed to high electric fields, with temperature probe data available. Therefore, a calibration for the temperature offset was performed. For this temperature calibration, the thermocouple probe measurements in the beakers were used (see the Materials and Methods section). Since temperatures derived from T_1 in ROI 1 and ROI 2 already corresponded to the measured probe temperatures, only the temperatures calculated from T_2 had to be calibrated. Figure 10a plots the full dataset, while Figure 10b–d shows the datasets for bulk, bridge base, and bridge, respectively. Due to the calibration procedure, the probe temperature and the T_1 and T_2 temperatures have to match for Figure 10b.

When comparing the temperatures in the other bridge sections to the probe measurements (Figure 10c,d), it is evident that measurements derived from T_2 show a tendency to overestimate the temperature. There is no significant discrepancy between the anode and cathode sides, and in all thermocouple and IR thermography recordings, both have

https://dx.doi.org/10.1021/acsomega.0c02059
ACS Omega XXXX, XXX, XXX–XXX

about the same temperature. Thus, the temperature derived from the T_1 time matches the probe recordings and those of previous thermographic recordings,[8] but T_2 overestimates the temperatures for ROIs 3 to 5.

As for Figure 9, it must be mentioned that in the bridge ROI measurement artifacts are likely. Local variations in voltage density ($\nabla^2 E \approx 10^{10}$ V · m^2) and different turbulences[36] should be mentioned apart from local temperature variations.[8]

The significance of the data is discussed in Figure 11 with the help of a Bland−Altman plot. In this plot, two different measurement procedures for the temperature are compared, each of which produced errors in measurement. While the data in the beakers are by definition in good correlation, the data from the bridge base and from the EHD bridge show a significant deviation in temperatures estimated from T_1 and T_2 times. In the EHD bridge, the voltage drop is highest (compared also to aqueous EHD bridges[7]) and so is the data shift between temperatures derived from T_1 and from T_2 times.

4.5. Discussion of T_1 and T_2 Variations in Electrically Stressed Glycerol. A recalculation of measured T_1 and T_2 times to the present temperatures using the calibration curves from Figure 8 should lead to a linear progression as any temperature-dependent changes, e.g., changes of chemical shifts,[50] are considered by experimental calibration curves. Hence, it is expected that the two derived temperatures will agree and should line up with the diagonal line in Figure 10. However, comparing T_1 and T_2 times measured in the EHD glycerol bridge clearly indicates that temperatures calculated from the T_2 times are slightly higher than the temperatures calculated from the T_1 times. Different changes of the chemical shifts of OH and alkyl protons caused by electrical voltage (3.5 kV) or flowing medium as well as concomitant changes in the excitation of the two proton species at high voltages cannot be held responsible as reasons for such deviations since such shift changes are marginal in EHD-driven glycerol (Figure 7).

Let us, hence, first assume that the applied electric field leads to a reduction of the averaged T_1 times and thus to incorrectly calculate temperatures. Such an influence cannot be ruled out, but in this experiment, such an effect is rather small since the temperatures from the T_1 times correspond to those measured by the probe (indicated by the cross in Figure 10). So, the results reveal that averaged T_1 relaxation times of glycerol will tend to provide a reasonably accurate estimation of temperature. It is therefore more likely that the T_2 times increase significantly due to the applied electric field (Figure 8b).

From a recent Raman study[7] and previous studies using femtosecond mid-infrared pump-probe spectroscopy,[32] we found that the electric field enhances proton conduction in EHD bridges made of water. Whenever an electric field is applied to a protic liquid, like glycerol, an increasing number of protons escape recombination as first discussed by Onsager and Brière.[51,52] Under HV, the dissociation rate is proportional to the electric field magnitude, but the recombination rate is not.[53,54] Such high electric fields can be found in the anode beaker enhancing the dissociation rate. The highest field gradients are found in the bridge and its bridge basis, which drives a proton current through the bridge.[7]

At the molecular level, this results in an increased mobility of the dissociated (positively charged) protons. These are in equilibrium between the dissociated and OH group bound forms with exchange rates, which are faster than the measuring time of a free induction decay in MRI. The quite well resolved, narrow ^{1}H signal of these protons at ca. 6.5 ppm in Figure 6b indicates this rapid exchange.[47] Consequently, the entropy of these protons becomes much larger due to the influence of the electric field than enthalpic changes. In the region near the extreme narrowing limit, this enhanced exchange rate leads to a reduction in the number of OH protons that precess with the Larmor frequency. Consequently, the relaxation times (T_1 and T_2) of these protons should noticeably increase.

This change in the relaxation times is mainly caused by the influence of the electric field on proton mobility due to the design of the EHD glycerol bridge apparatus, with virtually no electric current. From previous investigations in electrically stressed water,[4,13] we learned that when an HV is applied, such an increased proton mobility is caused by a dynamical coupling between the single molecule OH vibrations, leading to long-range phonon-like modes increasing proton conductivity. This quantum field effect drives the system out of thermal equilibrium and certainly will influence system entropy and spin−spin coupling in the way it is observed in Figures 9 and 10. The associated enthalpic effects (represented by the T_1 times) due to the heating and energy release to the thermal bath in all ROIs are represented by the calibration curves in Figure 8 and match quite well for MRI and NMR recordings. Hence, the influence of the electric field on the spin−lattice relaxation is small and the T_1 times are less affected.

Previously, we observed in an experiment with a free hanging glycerol bridge high velocities and fast fluctuations.[8] We now understand that entropic effects will cause protons to be more mobile when glycerol is electrically stressed compared to glycerol in the bulk. As with water, this higher proton mobility and stronger delocalization might have an effect on the physical properties of electrically stressed glycerol.

5. CONCLUSIONS

In a recent work, the authors observed the emergence of a new population in electrically stressed water that supports polarization currents.[5] In water, this leads to a higher proton mobility[13] and surface charges, which in turn reduce surface tension.[7]

In this work, another protonic liquid, glycerol, was tested under the influence of applied HV by 1.5 T MRI as well as at 9.4 T NMR with glycerol under no electric stress. NMR spectroscopy was used to confirm that MRI provides a reasonably accurate estimation of temperature. Under this premise, MRI enables the mapping of relative changes in T_1 and T_2 relaxation times when an HV is applied to the liquid, with the T_1 time providing a measure of the enthalpy of the system and the T_2 time representing the local entropy of the spin system.

When an HV is applied to glycerol, it turned out that associated effects in enthalpy are well represented by the temperature calibration curves recorded without HV applied, match quite well for MRI and NMR recordings, and represent energy released to the thermal bath. Hence, the influence of the electric field on the spin−lattice relaxation is small and the T_1 times are therefore less affected by the applied HV field.

On the contrary, the temperatures calculated from the T_2 times are significantly higher than the temperatures expected from the T_1 times. Thus, a smaller response of the spin−spin relaxation time T_2 on temperature is seen when an HV is applied to glycerol.

The authors conclude that these observations point toward a population of molecules in a glycerol EHD bridge where

https://dx.doi.org/10.1021/acsomega.0c02059
ACS Omega XXXX, XXX, XXX−XXX

protons are more mobile in the electrically stressed liquid compared to the glycerol in the bulk not affected by voltage. These results also support the hypothesis that, similar to water, this higher proton mobility and stronger delocalization might have an effect on the physical properties of electrically stressed glycerol, e.g., viscosity. Under the influence of HV, a change in physical properties in glycerol occurs, an effect similar to the one observed in electrically stressed water.[7]

AUTHOR INFORMATION

Corresponding Author

Elmar C. Fuchs − *Wetsus European Centre of Excellence for Sustainable Water Technology, Leeuwarden 8911MA, The Netherlands;* orcid.org/0000-0001-8632-2702; Email: elmar.fuchs@wetsus.nl

Authors

Adam D. Wexler − *Wetsus European Centre of Excellence for Sustainable Water Technology, Leeuwarden 8911MA, The Netherlands*

Jakob Woisetschläger − *Institute for Thermal Turbomachinery and Machine Dynamics, Working Group Metrology − Laser Optical Metrology, Graz University of Technology, Graz 8010, Austria*

Ursula Reiter − *Division of General Radiology, Department of Radiology, Medical University of Graz, Graz 8036, Austria*

Gert Reiter − *Division of General Radiology, Department of Radiology, Medical University of Graz, Graz 8036, Austria; Research & Development, Siemens Healthcare Diagnostics GmbH, Graz 8054, Austria*

Michael Fuchsjäger − *Division of General Radiology, Department of Radiology, Medical University of Graz, Graz 8036, Austria*

Lothar Brecker − *Department of Organic Chemistry, University of Vienna, 1090 Vienna, Austria*

Complete contact information is available at: https://pubs.acs.org/10.1021/acsomega.0c02059

Notes

The authors declare no competing financial interest.

ACKNOWLEDGMENTS

This work was performed at Wetsus, European Centre of Excellence for Sustainable Water Technology (www.wetsus.eu) and the Department of Radiology, Division of General Radiology, Medical University of Graz, Austria. Wetsus is co-funded by the Dutch Ministry of Economic Affairs and Ministry of Infrastructure and Environment, the Province of Fryslân, and the Northern Netherlands Provinces. The authors would like to thank the participants of the research theme "Applied Water Physics" for the fruitful discussions and their financial support.

REFERENCES

(1) Hertz, H. R. Ueber die Vertheilung der Electricität auf der Oberfläche bewegter Leiter. *Ann. Phys.* **1881**, *249*, 266−275.

(2) Quincke, G. Electrische Untersuchungen. VII, Ueber die Dielectricitätsconstanten isolirender Flüssigkeiten. *Ann. Phys Chem.* **1883**, *255*, 705−782.

(3) Armstrong, W. G. Electrical Phenomena. *The Electrical Engineer* **1893**, *10*, 154−155.

(4) Wexler, A. D.; Drusová, S.; Woisetschläger, J.; Fuchs, E. C. Non-equilibrium thermodynamics and collective vibrational modes of liquid water in an inhomogeneous electric field. *Phys. Chem. Chem. Phys.* **2016**, *18*, 16281−16292.

(5) Wexler, A. D.; Fuchs, E. C.; Woisetschläger, J.; Vitiello, G. Electrically induced liquid−liquid phase transition in water at room temperature. *Phys. Chem. Chem. Phys.* **2019**, *21*, 18541−18550.

(6) Fuchs, E. C.; Sammer, M.; Wexler, A. D.; Kuntke, P.; Woisetschläger, J. A floating water bridge produces water with excess charge. *J. Phys. D: Appl. Phys.* **2016**, *49*, 125502.

(7) Fuchs, E. C.; Yntema, D.; Woisetschläger, J. Raman spectroscopy and shadowgraph visualization of excess protons in high-voltage electrolysis of pure water. *J. Phys. D: Appl. Phys.* **2019**, *52*, 365302.

(8) Woisetschläger, J.; Wexler, A. D.; Holler, G.; Eisenhut, M.; Gatterer, K.; Fuchs, E. C. Horizontal bridges in polar dielectric liquids. *Exp. Fluids* **2012**, *52*, 193−205.

(9) Fuchs, E. C.; Wexler, A. D.; Agostinho, L. L. F.; Ramek, M.; Woisetschläger, J. Methanol, Ethanol and Propanol in EHD liquid bridging. *J. Phys. Conf. Ser.* **2011**, *329*, No. 012003.

(10) Teschke, O.; Mendez Soares, D.; Valente Filho, J. F. Floating liquid bridge tensile behavior: Electric-field-induced Young's modulus measurements. *Appl. Phys. Lett.* **2013**, *103*, 251608.

(11) Teschke, O.; Mendez Soares, D.; Gomes, W. E.; Valente Filho, J. F. Floating liquid bridge charge dynamics. *Phys. Fluids* **2016**, *28*, No. 012105.

(12) Marín, Á. G.; Lohse, D. Building water bridges in air: Electrohydrodynamics of the floating water bridge. *Phys. Fluids* **2010**, *22*, 122104.

(13) Fuchs, E. C.; Bitschnau, B.; Wexler, A. D.; Woisetschläger, J.; Freund, F. T. A Quasi-Elastic Neutron Scattering Study of the Dynamics of Electrically Constrained Water. *J. Phys. Chem. B* **2015**, *119*, 15892−15900.

(14) Gach, H. M. Technical Note: T_1 and T_2 and complex permittivities of mineral oil, silicone oil, and glycerol at 0.35, 1.5, and 3 T. *Med. Phys.* **2019**, *46*, 1785−1792.

(15) Segur, J. B.; Oberstar, H. E. Viscosity of Glycerol and its Aqueous Solutions. *Ind. Eng. Chem.* **1951**, *43*, 2117−2120.

(16) *International Association for the Properties of Water and Steam, "The International Association for the Properties of Water and Steam Revised Release on the IAPWS Industrial Formulation 1997 for the Thermodynamic Properties of Water and Steam"*, 2008, Lucerne, *Switzerland.*

(17) Claridge, T. D. W., *High-resolution NMR techniques in organic chemistry*; 3rd edn, Elsevier: Oxford, UK, 2016.

(18) Melcher, J. R.; Taylor, G. I. Electrohydrodynamics: A Review of the role of interfacial shear stresses. *Ann. Rev. Fluid Mech.* **1969**, *1*, 111−146.

(19) Melcher, J. R., *Continuum Electromechanics*; MIT Press: Cambridge, MA, 1981.

(20) Widom, A.; Swain, J.; Silverberg, J.; Sivasubramanian, S.; Srivastava, Y. N. Theory of the Maxwell pressure tensor and the tension in a water bridge. *Phys. Rev. E* **2009**, *80*, No. 016301.

(21) Burcham, C. L.; Saville, D. A. Electrohydrodynamic stability: Taylor-Melcher theory for a liquid bridge suspended in a dielectric gas. *J. Fluid Mech.* **2002**, *452*, 163−187.

(22) Ramos, A.; Castellanos, A. Bifurcation diagrams of axisymetric liquid bridges of arbitrary volume in electric and gravitational axial fields. *Phys. Fluids* **1993**, *249*, 207−225.

(23) Fuchs, E. C.; Woisetschläger, J.; Gatterer, K.; Maier, E.; Pecnik, R.; Holler, G.; Eisenkölbl, H. The floating water bridge. *J. Phys. D: Appl. Phys.* **2007**, *40*, 6112−6114.

(24) Sammer, M.; Wexler, A. D.; Kuntke, P.; Wiltsche, H.; Stanulewicz, N.; Lankmayr, E.; Woisetschläger, J.; Fuchs, E. C. Proton production, neutralisation and reduction in a floating water bridge. *J. Phys. D: Appl. Phys.* **2015**, *48*, 415501.

(25) Fuchs, E. C.; Cherukupally, A.; Paulitsch-Fuchs, A. H.; Agostinho, L. L. F.; Wexler, A. D.; Woisetschläger, J.; Freund, F. T. Investigation of the Mid-Infrared Emission of a Floating Water Bridge. *J. Phys. D: Appl. Phys.* **2012**, *45*, 475401.

(26) Wexler, A. D.; López Sáenz, M.; Schreer, O.; Woisetschläger, J.; Fuchs, E. C. The preparation of electrohydrodynamic bridges from polar dielectric liquids. *J. Visualized Exp.* **2014**, *91*, e51819.
(27) Skinner, L. B.; Benmore, C. J.; Shyam, B.; Weber, J. K. R.; Parise, J. B. Structure of the floating water bridge and water in an electric field. *Proc. Natl. Acad. Sci. U. S. A.* **2012**, *109*, 16463−16468.
(28) Fuchs, E. C.; Bitschnau, B.; Woisetschläger, J.; Maier, E.; Beuneu, B.; Teixeira, J. Neutron Scattering of a Floating Heavy Water Bridge. *J. Phys. D: Appl. Phys.* **2009**, *42*, No. 065502.
(29) Fuchs, E. C.; Baroni, P.; Bitschnau, B.; Noirez, L. Two-dimensional neutron scattering in a floating heavy water bridge. *J. Phys. D: Appl. Phys.* **2010**, *43*, 105502.
(30) Fuchs, O.; Zharnikov, M.; Weinhardt, L.; Blum, M.; Weigand, M.; Zubavichus, Y.; Bär, M.; Maier, F.; Denlinger, J. D.; Heske, C.; Grunze, M.; Umbach, E. Isotope and temperature effects in liquid water probed by X-ray absorption and resonant X-ray emission spectroscopy. *Phys. Rev. Lett.* **2008**, *100*, 249802.
(31) Fuchs, E. C.; Bitschnau, B.; Di Fonzo, S.; Gessini, A.; Woisetschläger, J. Inelastic UV scattering in a floating water bridge. *J. Phys. Sci.Appl.* **2011**, *1*, 135−147.
(32) Piatkowski, L.; Wexler, A. D.; Fuchs, E. C.; Schoenmaker, H.; Bakker, H. J. Ultrafast vibrational energy relaxation of the water bridge. *Phys. Chem. Chem. Phys.* **2012**, *14*, 6160−6164.
(33) Ponterio, R. C.; Pochylski, M.; Aliotta, F.; Vasi, C.; Fontanella, M. E.; Saija, F. Raman scattering measurements on a floating water bridge. *J. Phys. D: Appl. Phys.* **2010**, *43*, 175405.
(34) Levitt, M. H., *Spin dynamics: Basics of nuclear magnetic resonance*;2nd edn, Wiley: Oxford, UK, 2008.
(35) Bloch, F. Nuclear Induction. *Phys. Rev.* **1946**, *70*, 460−474.
(36) Wexler, A. D.; Drusová, S.; Fuchs, E. C.; Woisetschläger, J.; Reiter, G.; Fuchsjäger, M.; Reiter, U. Magnetic resonance imaging of flow and mass transfer in electrohydrodynamic liquid bridges. *J. Vis.* **2017**, *20*, 97.
(37) Hintze, J. (2008). PASS 2008. *NCSS, LLC*. Kaysville, Utah, USA. www.ncss.com.
(38) Bernstein, M.; King, K.; Zhou, X., *Handbook of MRI Pulse Sequences;* Elsevier: Burlington, MA, USA, 2004.
(39) Brecker, L.; Pogorevc, M.; Griengl, H.; Steiner, W.; Kappe, T.; Ribbons, D. W. Synthesis of 2,4-diketo acids and their aqueous solution structures. *New J. Chem.* **1999**, *23*, 437−446.
(40) Berger, S.; Braun, S., *200 and More NMR Experiments;* 3rd edn. Wiley-VCH: Weinheim, Germany, 2004.
(41) Gottlieb, H. E.; Kotlyar, V.; Nudelman, A. NMR chemical shifts of common laboratory solvents as trace impurities. *J. Org. Chem.* **1997**, *62*, 7512−7515.
(42) Vold, R. L.; Waugh, J. S.; Klein, M. P.; Phelps, D. E. Measurement of spin relaxation to complex systems. *J. Chem. Phys.* **1968**, *48*, 3831−3832.
(43) Carr, H. Y.; Purcell, E. M. Effects of diffusion on free precession in nuclear magnetic resonance experiments. *Phys. Rev.* **1954**, *94*, 630−638.
(44) Meiboom, S.; Gill, D. Modified spin-echo method for measuring nuclear relaxation times. *Rev. Sci. Instrum.* **1958**, *29*, 688−691.
(45) Noack, F.; Preissing, G. Magnetische Relaxation in Glycerin. *Z. Naturforsch.* **1969**, *24*, 143−153.
(46) Noack, F.; Preissing, G.; Kosfeld, R.; Gross, B. On the proton spin relaxation in glycerol. *Z. Phys.* **1971**, *246*, 84−90.
(47) Sudmeier, J. L.; Anderson, S. E.; Frye, J. S. Calculations of nuclear spin relaxation times. *Concepts Magn. Reson.* **1990**, *2*, 197−212.
(48) Frahm, J.; Merboldt, K.-D.; Hänicke, W. Localized proton spectroscopy using stimulated echoes. *J. Magn. Reson.* **1987**, *72*, 502−508.
(49) Thompson, R. B.; Allen, P. S. Response of metabolites with coupled spins to the STEAM sequence. *Magn. Reson. Med.* **2001**, *45*, 955−965.
(50) Bielejewski, M. J. Effect of self-assembly aggregation on physical properties of non-aqueous ionogels based on LMWG. *J. Sol-Gel Sci. Technol.* **2018**, *88*, 671−683.
(51) Onsager, L. Deviations from Ohm's law in weak electrolytes. *J. Chem. Phys.* **1934**, *2*, 599−615.
(52) Briere, G. B. Electrical conduction in purified polar liquids. *Brit. J. Appl. Phys.* **1964**, *15*, 413−417.
(53) Zhakin, A. I., Conduction phenomena in dielectric liquids. in *Electrohydrodynamics, International Centre for Mechanical Sciences, CISM Courses and Lectures No. 380*; Castellanos, A. (ed) Springer: Vienna, 1998.
(54) Jeong, S. I.; Seyed-Yagoobi, J.; Atten, P. Theoretical/numerical study of electrohydrodynamic pumping through conduction phenomenon. *IEEE Trans. Ind. Appl.* **2003**, *39*, 355−361.

https://dx.doi.org/10.1021/acsomega.0c02059
ACS Omega XXXX, XXX, XXX−XXX